PHOTONICS Research

# Creation of cylindrical vector beams through highly anisotropic scattering media with a single scalar transmission matrix calibration

Qian Zhao,[1] Shijie Tu,[1] Qiannan Lei,[1] Chengshan Guo,[1,4] Qiwen Zhan,[2,5] and Yangjian Cai[1,3,6]

[1]Shandong Provincial Engineering and Technical Center of Light Manipulations & Shandong Provincial Key Laboratory of Optics and Photonic Device, School of Physics and Electronics, Shandong Normal University, Jinan 250358, China
[2]School of Optical-Electrical and Computer Engineering, University of Shanghai for Science and Technology, Shanghai 200093, China
[3]School of Physical Science and Technology, Soochow University, Suzhou 215006, China
[4]e-mail: guochsh@sdnu.edu.cn
[5]e-mail: qwzhan@usst.edu.cn
[6]e-mail: yangjiancai@sdnu.edu.cn

Received 14 March 2022; revised 7 May 2022; accepted 11 May 2022; posted 16 May 2022 (Doc. ID 457928); published 21 June 2022

**Cylindrical vector (CV) beams have attracted increasing interest due to their particular properties and their applications in optical imaging, optical manipulation, and light–matter interactions. However, it is challenging to construct CV beams through highly anisotropic scattering media (HASM), such as thick biological tissue, posing a barrier to the applications of CV beams that involve HASM. Here, we present a scheme to construct CV beams beyond high scattering that only requires a single scalar transmission matrix (TM) calibration and manipulation of the spatial degrees of freedom of the scalar input field. Assisted by a radial polarization converter (S-waveplate) and a polarizer, the scheme enables one to obtain the correct incident wavefront for the creation of CV beams through HASM with only one single scalar TM calibration. Compared to the existing method, this user-friendly approach is fast and simple in terms of the optical implements and computations. Both radially and azimuthally polarized beams are experimentally constructed through a ZnO scattering layer to demonstrate the viability of the method. Arbitrarily generalized CV beams and arrays of CV beams are also created through the HASM to further prove the flexibility of the method. We believe this work may pave the way for applications of CV beams that involve a highly anisotropic scattering environment.** © 2022 Chinese Laser Press

https://doi.org/10.1364/PRJ.457928

## 1. INTRODUCTION

Optical vector fields may possess singularities associated with the parameterization of elliptical and partial polarization rather than phase [1]. For example, cylindrical vector (CV) beams with cylindrical polarization symmetry contain an undefined polarization azimuth at the center [2,3]. The peculiar polarization symmetry of CV beams gives rise to unique properties under high-numerical-aperture focusing [2,4,5], which has attracted much attention in fields such as superresolution imaging [6,7], optical trapping [8–10], laser materials processing [11], and light–matter interactions [12,13]. Since 1972 [14,15], many methods have been developed to produce CV beams, including using laser intracavity devices [14,15] that force the laser to oscillate in CV modes, polarization manipulation with spatial light modulators (SLMs) [16–18], and employing space variant polarization converters [19–21]. However, all of these studies are typically implemented in free space and experience little or no sample aberrations.

Light propagation in media with inhomogeneous index distributions suffers scattering. In highly anisotropic scattering media (HASM) such as white paint, biological tissue, and multimode fiber, the degrees of freedom of the incident beams including amplitude, phase, and polarization are completely scrambled due to multiple scattering [22–24]. In this case, the applications of CV beams behind the HASM are greatly restrained. To overcome the scattering, wavefront shaping techniques such as iterative optimization [25–27], optical phase conjugation [28,29], and the transmission matrix (TM) method [30–34] have opened the possibility to achieve light control through HASM. For example, an optimized input field obtained by optimizing the intensity of a target focal position enables scattered light propagating along different paths to interfere constructively at the target position, and thus a focus is shaped beyond scattering. A phase conjugation mirror, such as a specially prepared photorefractive crystal, can be used to record the wavefront of the scattered light from a target location in a hologram and then phase conjugate the light back to the target

location, therefore generating a focus. Besides, for a scattering medium, the relationship between the input light and the output light can be characterized by a TM. A well-calibrated TM enables the light transporting through the HASM to form the target light field. Moreover, with a trained neural network, deep-learning-based algorithms have shown their great potential in predicting the correct incident field for shaping a desired intensity distribution behind the scattering media [35–37]. Apart from the intensity modulation through scattering media, deep-learning-based algorithms may also be expected to control the polarization degree of freedom beyond scattering.

In a nutshell, the desired light field can be shaped through HASM as long as taking the correct incident wavefront as the input field. However, to obtain the correct incident wavefront for creating CV beams with variant polarization distributions in space through HASM, the existing method [31,34] commonly requires calibration of the vector transmission matrix (VTM) of the HASM that contains four scalar TMs, and inverts it to find the vector input field. Thus this method needing to measure the four scalar TMs and simultaneously manipulate both the spatial and polarization degrees of freedom at the input field consumes much time, needs complex calculations, and relies on a complicated experimental setup.

To address this issue, we present a fast and simple method to construct CV beams through HASM, which only relies on modulation in the spatial degrees of freedom of the scalar input field and calibration of a single scalar TM. Compared to the existing method, our method costs a short time, implements with a simplified optical design, and does not need complex calculations. To shape CV beams through HASM, a radial polarization converter (S-waveplate), which is fabricated by a femtosecond laser writing of self-assembled nanostructures in silica glass [19], and a polarizer are employed in the process of TM calibration. The correct incident wavefront for constructing a CV beam through HASM is obtained by only one single scalar TM calibration. Experimentally, both radially and azimuthally polarized beams are constructed through a ZnO scattering layer. To verify their polarization states, their polarization maps are derived from the first three elements of Stokes parameters. Further, we demonstrate that arbitrarily generalized CV beams can be produced through the ZnO scattering layer by changing the direction of the polarizer. In addition, three arrays of CV beams are generated through the ZnO scattering layer. Our work will promote the applications that rely on CV beams through HASM.

## 2. PRINCIPLE AND EXPERIMENTAL SETUP

### A. Principle of Constructing CV Beams through HASM with a Single Scalar TM Calibration

Figure 1 illustrates the principle of constructing CV beams through HASM with a single scalar TM calibration. As shown in Fig. 1(a), when a linearly polarized beam is incident on a HASM, its state of polarization is scrambled by multiple scattering as well as the amplitude and phase distribution. As a result, the transmitted light is turned into arbitrary intensity speckles with randomly distributed polarization states at the output plane. According to the VTM method, the relationship between the output field $E_{\text{out}}$ (divided into $P \times Q$ output

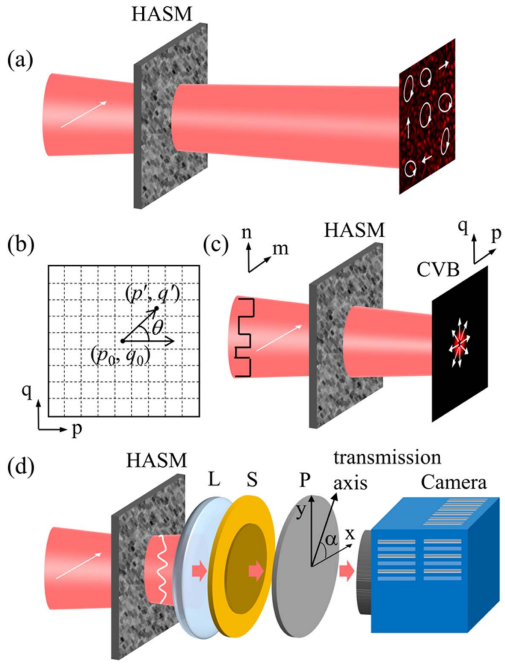


**Fig. 1.** Principle of constructing CV beams through HASM with a single scalar TM calibration. (a) Multiple scattering scrambles the wavefront of the incident linearly polarized beam, and the transmitted light is composed of all spatial modes in different polarization states. (b) Definition of the output coordinates. (c) A CV beam can be produced through HASM with the input field reshaped according to Eq. (3). (d) Principal schematic of TM calibration to shape CV beams through HASM with a single scalar TM calibration. HASM, highly anisotropic scattering medium; L, lens; S, S-waveplate; P, polarizer; CVB, cylindrical vector beam.

modes) and input field $E_{\text{in}}$ (divided into $M \times N$ input modes), which are respectively defined at the coordinates $(p, q)$ and $(m, n)$, can be described by

$$\begin{aligned}\mathbf{E}_{\text{out}}(p,q) &= \begin{bmatrix} E_{\text{out},x}(p,q) \\ E_{\text{out},y}(p,q) \end{bmatrix} \\ &= \sum_{m,n} \begin{bmatrix} T_{xx}(m,n,p,q) & T_{yx}(m,n,p,q) \\ T_{xy}(m,n,p,q) & T_{yy}(m,n,p,q) \end{bmatrix} \begin{bmatrix} E_{\text{in},x}(m,n) \\ E_{\text{in},y}(m,n) \end{bmatrix}, \end{aligned} \quad (1)$$

where $T_{ij}(m, n, p, q)$ is the matrix element of the VTM and represents the complex amplitude of the $j$-polarized component of the output mode $(p, q)$ resulting from the $i$-polarized component of the input mode $(m, n)$. In this case, the VTM contains four scalar complex components. When the full VTM is known, the arbitrary CV beams with the desired spatial distribution and polarization state can be shaped through the HASM in theory [33]. However, to control the polarization of the transmitted light, it is not necessary to calibrate both polarization components. With the randomness of the scattering medium providing sufficient polarization diversity, the calibration of the VTM elements corresponding to one of the polarization inputs is adequate to achieve this goal [38]. Supposing the input field is a linearly polarized beam along the $x$ direction, Eq. (1) can be simplified as

$$\begin{aligned}\mathbf{E}_{\text{out}}(p,q) &= \sum_{m,n}\begin{bmatrix} T_{xx}(m,n,p,q) & T_{yx}(m,n,p,q) \\ T_{xy}(m,n,p,q) & T_{yy}(m,n,p,q)\end{bmatrix}\begin{bmatrix} E_{\text{in},x}(m,n) \\ 0\end{bmatrix} \\ &= \sum_{m,n} E_{\text{in},x}(m,n)\begin{bmatrix} T_{xx}(m,n,p,q) \\ T_{xy}(m,n,p,q)\end{bmatrix}. \end{aligned} \tag{2}$$

If the input beam is further set to be

$$\begin{aligned}E_{\text{in},x}(m,n) = \sum_{p',q'}[&\cos\theta(p'-p_0,q'-q_0)\,T^*_{xx}(m,n,p',q') \\ &+ \sin\theta(p'-p_0,q'-q_0)\,T^*_{xy}(m,n,p',q')],\end{aligned} \tag{3}$$

then Eq. (2) can be expressed as

$$\mathbf{E}_{\text{out}}(p,q) = \sum_{m,n} E_{\text{in},x}(m,n)\begin{bmatrix} T_{xx}(m,n,p,q) \\ T_{xy}(m,n,p,q)\end{bmatrix} = \sum_{m,n}\begin{bmatrix} \sum_{p',q'}[\cos\theta(p'-p_0,q'-q_0)\,T^*_{xx}(m,n,p',q')\,T_{xx}(m,n,p,q) \\ +\sin\theta(p'-p_0,q'-q_0)\,T^*_{xy}(m,n,p',q')\,T_{xx}(m,n,p,q)] \\ \sum_{p',q'}[\cos\theta(p'-p_0,q'-q_0)\,T^*_{xx}(m,n,p',q')\,T_{xy}(m,n,p,q) \\ +\sin\theta(p'-p_0,q'-q_0)\,T^*_{xy}(m,n,p',q')\,T_{xy}(m,n,p,q)]\end{bmatrix}. \tag{4}$$

In Eqs. (3) and (4), '$*$' stands for the conjugate operation, $(p_0,q_0)$ are the coordinates of an interested position at the output plane, and $\theta$ is the polar angle of the polar coordinates of a point $(p',q')$ relative to the interested point $(p_0,q_0)$, that is, $\theta = \arctan[(q'-q_0)/(p'-p_0)]$. The definition of the output coordinates is sketched in Fig. 1(b).

Each VTM element of a HASM can be considered as a random complex function of both the coordinates $(m,n)$ and $(p,q)$, and the sum of their product can be simplified as

$$\begin{aligned}&\sum_{m,n} T^*_{xx}(m,n,p',q')\,T_{xx}(m,n,p,q) \\ &= \sum_{m,n} T^*_{xy}(m,n,p',q')\,T_{xy}(m,n,p,q) \\ &\approx \begin{cases}\varepsilon_0, & \text{for } p'=p, q'=q \\ \varepsilon_1, & \text{for } p'\neq p, q'\neq q\end{cases},\end{aligned} \tag{5}$$

and

$$\begin{aligned}&\sum_{m,n} T^*_{xy}(m,n,p',q')\,T_{xx}(m,n,p,q) \\ &= \sum_{m,n} T^*_{xx}(m,n,p',q')\,T_{xy}(m,n,p,q) \approx \varepsilon_2.\end{aligned} \tag{6}$$

The probability theory shows that the module of $\varepsilon_0$ is $\sqrt{M\times N}$ times larger than that of $\varepsilon_1$ or $\varepsilon_2$ [39]. Obviously, when the input mode number $M\times N$ is large enough, $\varepsilon_1$ and $\varepsilon_2$ will be much smaller than $\varepsilon_0$. For example, if $M\times N$ is set to $32\times 32$, as is used in our experiments, the module size of $\varepsilon_1$ or $\varepsilon_2$ is only about 3% of $\varepsilon_0$. In this case, Eq. (4) can be approximately expressed as

$$\mathbf{E}_{\text{out}}(p,q) \approx \varepsilon_0\begin{bmatrix}\cos\theta(p-p_0,q-q_0) \\ \sin\theta(p-p_0,q-q_0)\end{bmatrix}. \tag{7}$$

Equation (4) and its approximation Eq. (7) reveal that we can generate a radially polarized beam with its center located at the output mode $(p_0,q_0)$ through the HASM [as shown in Fig. 1(c)] as long as the input field is reshaped according to Eq. (3), in which two elements of the VTM are required.

Here we further propose a single-step measurement method to determine the two elements of the VTM required for the reshaped input field shown in Eq. (3). Figure 1(d) is the principal schematic of the calibration process, in which a spatially variant half-wave plate (S-waveplate) [40] and a polarizer are used. In the process, the S-waveplate is located at the exit pupil plane of the imaging lens that is employed to magnify and image the transmitted speckle field to the camera plane. In this case, the equivalent effect of the S-waveplate is a spatial polarization filter of the VTM. Thus the field at a position $(p,q)$ of the output plane can be seen as a convolution between the Jones matrix of the S-waveplate and the transmitted speckle field of the HASM. Supposing the input field is a linearly polarized beam along the $x$ direction, the orientation of the S-waveplate is set along the $x$ axis and the angle between the transmission axis of the polarizer and the $x$ axis is $\alpha$. With this configuration, the complex amplitude distribution recorded by the image sensor when a single input point source $E_{\text{in},x}(m,n)$ is taken as the input field can be written as

$$\begin{aligned}E^{\text{calib}}_{\text{out}}(m,n,p,q,\alpha) &= P(\alpha)\begin{bmatrix}\cos\theta(p,q) & \sin\theta(p,q) \\ \sin\theta(p,q) & -\cos\theta(p,q)\end{bmatrix} \\ &\otimes\begin{bmatrix} T_{xx}(m,n,p,q) & T_{yx}(m,n,p,q) \\ T_{xy}(m,n,p,q) & T_{yy}(m,n,p,q)\end{bmatrix}\begin{bmatrix} E_{\text{in},x}(m,n) \\ 0\end{bmatrix} \\ &= \cos\alpha\sum_{p',q'} E_0[\cos\theta(p'-p,q'-q)\,T_{xx}(m,n,p',q') \\ &\quad + \sin\theta(p'-p,q'-q)\,T_{xy}(m,n,p',q')] \\ &\quad + \sin\alpha\sum_{p',q'} E_0[\sin\theta(p'-p,q'-q)\,T_{xx}(m,n,p',q') \\ &\quad - \cos\theta(p'-p,q'-q)\,T_{xy}(m,n,p',q')] \\ &= \sum_{p',q'} E_0[\cos\alpha\cos\theta(p'-p,q'-q) \\ &\quad + \sin\alpha\sin\theta(p'-p,q'-q)]\,T_{xx}(m,n,p',q') \\ &\quad + \sum_{p',q'} E_0[\cos\alpha\sin\theta(p'-p,q'-q) \\ &\quad - \sin\alpha\cos\theta(p'-p,q'-q)]\,T_{xy}(m,n,p',q'),\end{aligned} \tag{8}$$

where the field of every input mode is set as the same constant $E_0$ and '$\otimes$' represents convolution operation. $E_{\text{out}}^{\text{calib}}(m,n,p_0,q_0,\alpha)$ is the speckle field of the scattering system constituted by the HASM, the imaging lens, the S-waveplate, and the polarizer, and thus it can be directly determined by calibrating the scalar TM of this scattering system. Obviously, as long as the field of $E_{\text{out}}^{\text{calib}}(m,n,p_0,q_0,\alpha)$ is measured, the required input field for generating a CV beam through the HASM centered at the output mode $(p_0,q_0)$ can be obtained simply by a conjugate operation, that is,

$$E_{\text{in},x}(m,n) = [E_{\text{out}}^{\text{calib}}(m,n,p_0,q_0,\alpha)]^*. \tag{9}$$

For example, when $\alpha = 0$, the required input field for generating a radially polarized beam as given in Eq. (7) can be obtained. Through a similar deduction process described above it can be derived that, if the input filed is set by Eq. (9) with $\alpha = \pi/2$, the output field will be converted into

$$\mathbf{E}_{\text{out}}(p,q) \approx \varepsilon_0 \begin{bmatrix} \sin\theta(p-p_0,q-q_0) \\ -\cos\theta(p-p_0,q-q_0) \end{bmatrix}, \tag{10}$$

which indicates the established field is an azimuthally polarized beam. Further, if $\alpha$ is an arbitrary angle, the resulting output field can be generally expressed as

$$\mathbf{E}_{\text{out}}(p,q) \approx \varepsilon_0 \left( \cos\alpha \begin{bmatrix} \cos\theta(p-p_0,q-q_0) \\ \sin\theta(p-p_0,q-q_0) \end{bmatrix} + \sin\alpha \begin{bmatrix} \sin\theta(p-p_0,q-q_0) \\ -\cos\theta(p-p_0,q-q_0) \end{bmatrix} \right). \tag{11}$$

As we can see, the generated output field is a generalized CV beam [5]. Compared to the radially polarized beam, each point of this beam possesses a polarization that is rotated by $\alpha$ from the radial direction. The coefficients $\cos\alpha$ and $\sin\alpha$ ($\alpha \in [0,\pi]$) are the weighting factors that allow a smooth transition of the constructed light beam from radially polarized beam ($\alpha = 0,\pi$) to azimuthally polarized beam ($\alpha = \pi/2$). In this case, generalized CV beams can be generated through HASM flexibly by adjusting the direction of the polarizer.

### B. Experimental Setup

In order to validate our proposal, we built an experimental setup, which is schematically shown in Fig. 2(a). To achieve wavefront shaping, a digital micro-mirror device [27,41,42] (DMD, Vialux V-7001) was employed as the SLM. A laser beam from a laser ($\lambda = 532$ nm, Cobolt 04-01 Series) was expanded by a telescope (constituted by L1 and L2) and steered by M1 to pass BS1. After that the beam was divided into two parts; the transmitted beam was signal light and fully illuminated the surface of the DMD, while the reflected beam was then redirected by M2, M3, and BS2 to perform as a reference beam. With the help of a $4f$ configuration (constituted by L3 and L4) and a spatial filter, Lee method [43] enabled the DMD to modulate the complex amplitude of light in its first-diffraction-order beam. Then the modulated beam impinged on a deposited ZnO scattering layer via an objective O1 (10×, NA = 0.25) and underwent multiple scattering when propagating in it. A ZnO scattering layer with thickness of about 200 μm was used here as a HASM, whose photo is shown in Fig. 2(b). The distance between the ZnO scattering layer and the focal plane was about 200 μm. Then the resultant light field

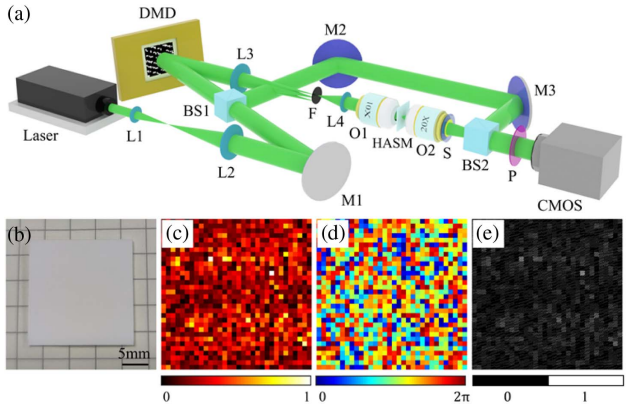


**Fig. 2.** Experimental scheme. (a) Experimental setup. L, lens; M, mirror; BS, beam splitter; DMD, digital micro-mirror device; F, filter; O, objective; HASM, highly anisotropic scattering medium; S, S-waveplate; P, polarizer; CMOS, complementary metal-oxide-semiconductor camera. (b) Photo of the HASM (a ZnO scattering layer) used. (c), (d) Amplitude and phase distributions of the correct incident field for constructing a radially polarized beam through the HASM. (e) Corresponding binary amplitude mask calculated by Lee method.

was collected by another objective O2 (20×, NA = 0.4) and imaged by a CMOS camera (D752, PixeLINK). To implement our scheme, an S-waveplate (RPC-532-06, Altechna R&D) was placed at the exit pupil plane of O2 and a polarizer was placed in front of the CMOS camera.

To calibrate the TM, a phase shifting method [30] was applied. In the TM calibration, each of the input modes was turned on sequentially with the rest turned off, and the corresponding transmitted speckle field was measured from interferometric measurements where the signal light was introduced with four predetermined phase shifts. By making measurements for all input modes, the corresponding elements of the transmission matrix were calibrated in sequence. In the calibration, $32 \times 32$ input segments on the DMD and $480 \times 480$ pixels on the camera were respectively used as the input and output modes, and the Hadamard basis was adopted to gain a high signal-to-noise ratio.

## 3. RESULTS

### A. Construct Radially and Azimuthally Polarized Beams through the ZnO Scattering Layer

We first experimentally constructed a radially and an azimuthally polarized beams through the ZnO scattering layer. To construct a radially polarized beam, the transmission axis of polarizer is set to be parallel with the $x$ axis in the process of TM calibration. After the conjugation of the calibrated TM was employed, one correct incident field was calculated, whose amplitude and phase distributions are respectively presented in Figs. 2(c) and 2(d). Then a binary amplitude mask encoding the complex input field was obtained by using Lee method and is shown in Fig. 2(e). With the binary amplitude mask displayed on the DMD, we obtained a bright focus at the plane of the CMOS camera, whose intensity pattern is shown in Fig. 3(a). To investigate the field distribution behind the ZnO layer, we removed the S-waveplate and the polarizer.

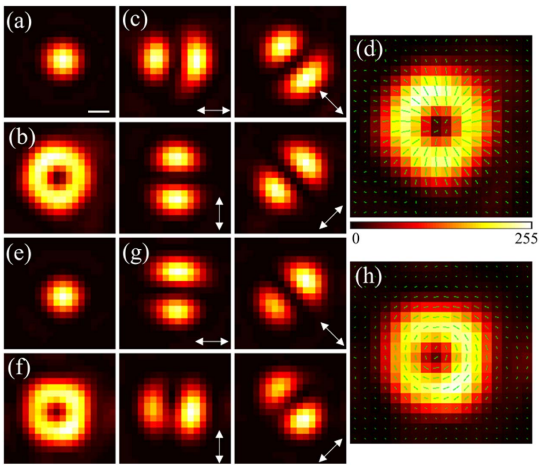


**Fig. 3.** Construct radially polarized and azimuthally polarized beams through the ZnO scattering layer. (a) Intensity pattern of the focus at the plane of CMOS camera when the S-waveplate and polarizer are still located in the optical path. (b) Observed intensity distribution of a radially polarized beam with the S-waveplate and the polarizer removed. (c) Fields after a polarizer whose transmission axis orientation is indicated by the white arrows at 0°, 45°, 90°, and 135°, respectively. (d) Intensity distribution of the radially polarized beam superimposed with the polarization map. The local polarization direction and the local intensity are indicated by the orientation of the lines and the length of lines, respectively. (e)–(h) Corresponding results for creating an azimuthally polarized beam. Scale bar: 20 μm.

Then we observed a donut beam at the imaging plane, whose intensity pattern is shown in Fig. 3(b). To characterize the polarization property of the beam, its corresponding experimental intensity profiles, acquired by passing it through a linear polarizer, are shown in Fig. 3(c). The white arrows indicate the directions of the linear polarizer. Then in order to further quantify the polarization distribution of the beam, its polarization map [Fig. 3(d)] was calculated based on the first three elements of Stokes parameters, i.e., $S_0$, $S_1$, and $S_2$ [17]. The three parameters were deduced by measuring the intensities at each point of the distributions in Fig. 3(c). The local polarization direction whose angular orientation was calculated by $1/2\arctan(S_2/S_1)$ and the local intensity calculated by $\sqrt{2(S_0+\sqrt{S_1^2+S_2^2})}$ [44] are indicated by the orientation of the lines and the length of the lines, respectively. In the polarization map, radial polarization in the donut beam is observed and the spatially variant polarization rotation capability is demonstrated. Further, we generated an azimuthally polarized beam through the ZnO scattering layer by setting the transmission axis of the polarizer to be perpendicular to the $x$ axis in the process of TM calibration, and the corresponding experimental results are presented in Figs. 3(e)–3(h). Similarly, as we can see, the donut beam with the desired azimuthally polarized distribution was constructed through the ZnO scattering layer by using our proposed method.

### B. Construct Generalized CV Beams through the ZnO Scattering Layer

Apart from the radially and azimuthally polarized beams, generalized CV beams possess the particular focusing property [5]. Therefore, in order to promote the applications of generalized CV beams behind HASM, we explored the construction of the generalized CV beams beyond high scattering. Here, four generalized CV beams were produced through the ZnO scattering layer by changing the direction of the polarizer. Note that the angle between the transmission axis of the polarizer and the $x$ axis, $\alpha$, was set as $\pi/8$, $\pi/4$, $3\pi/4$, and $7\pi/8$, respectively. The intensity fields of the constructed CV beams were analyzed by a polarizer, and are correspondingly presented in Figs. 4(a)–4(d). To quantify the polarization manipulation ability of our method, the intensity patterns of the generated CV beams superimposed with their polarization maps are correspondingly shown in Figs. 4(a′)–4(d′). As we can see, the symmetry of the polarization distribution can be easily manipulated by adjusting the parameter $\alpha$. In this case, an arbitrarily generalized CV beam through HASM can be created flexibly by using this method.

### C. Construct Arrays of CV Beams through the ZnO Scattering Layer

In addition to constructing a single CV beam through the ZnO scattering layer, the arrays of CV beams can be shaped. With the proposed method, a single desired CV beam can be constructed through HASM by impinging the correct incident field for focusing at a predetermined output mode on HASM. To generate multiple CV beams through HASM, correct incident fields $E^1_{\text{in},x}, E^2_{\text{in},x}, \ldots,$ and $E^i_{\text{in},x}$ corresponding to focusing at different output modes with coordinates $(p_1, q_1)$, $(p_2, q_2)$, …, $(p_i, q_i)$ were precalculated, respectively. According to the uncorrelation between the different elements of the TM and the linearity of the scattering process [45], incidence of a superimposed input field, which is the sum of $E^1_{\text{in},x}, E^2_{\text{in},x}, \ldots, E^i_{\text{in},x}$ on HASM, could produce CV beams through HASM at the output modes of $(p_1, q_1), (p_2, q_2), \ldots, (p_i, q_i)$ simultaneously. First, an array of radially polarized beams and an array of azimuthally polarized beams were generated, respectively. Their intensity patterns and the fields passing through a polarizer are presented in Figs. 5(a) and 5(b), respectively. As we can see, each of the CV beams in the arrays was well shaped and carried the desired polarization state. Further, as shown in Fig. 5(c), we were also capable of constructing an array of

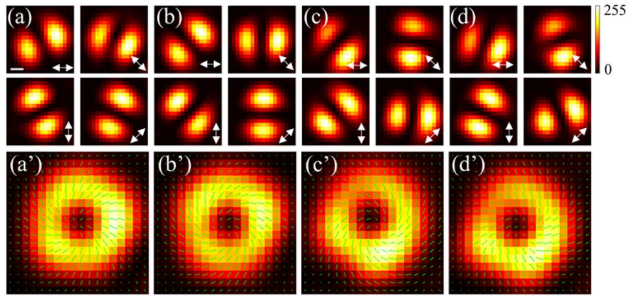


**Fig. 4.** Construct arbitrarily generalized CV beams through the ZnO scattering layer. (a)–(d) Fields after a polarizer whose transmission axis orientation is indicated by the white arrows at 0°, 45°, 90°, and 135°, respectively. For the four generated CV beams, $\alpha = \pi/8$, $\pi/4$, $3\pi/4$, and $7\pi/8$, respectively. (a′)–(d′) The intensity distribution of the generated CV beams superimposed with their polarization maps. Scale bar: 20 μm.

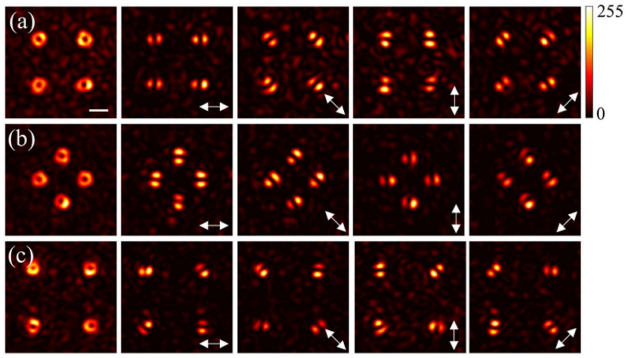


**Fig. 5.** Construct arrays of CV beams through the ZnO scattering layer. (a) Construct an array of radially polarized beams and the fields after a polarizer whose transmission axis orientation is indicated by the white arrows at 0°, 45°, 90°, and 135°, respectively. (b) Corresponding results of generating an array of azimuthally polarized beams. (c) Corresponding results of producing an array of CV beams with different polarization states. Here, for the four beams located on the upper left, the upper right, the bottom left, and the bottom right in the observation plane, $\alpha$ was respectively set as 0, $3\pi/4$, $\pi/4$, and $\pi/2$. Scale bar: 100 μm.

CV beams, in which the constituted CV beams are with different polarization states, by superposing their correct incident wavefronts together. Here, for the four beams that are located on the upper left, the upper right, the bottom left, and the bottom right in Fig. 5(c), $\alpha$ was respectively set as 0, $3\pi/4$, $\pi/4$, and $\pi/2$. As we can see, all of the polarization states of CV beams were well shaped. With the presented method, the numbers and the locations of the CV beams can be flexibly tuned by changing the numbers and positions of the predetermined output modes in the conjugation operation. The constructed arrays of CV beams could be beneficial to parallel trapping and manipulation of a number of microparticles through HASM.

## 4. DISCUSSION AND CONCLUSION

We have proposed a simple method to generate CV beams through HASM. For the method of generating CV beams through HASM with VTM calibration [31,34], the target vector output field is defined by the complex field of the desired CV beam; thus the size of the desired CV beam can be user-defined by setting its range in the output coordinates. In comparison, our method does not tailor the size of generated CV beams with such flexibility. The generated field in our method is actually a focus with the form of a CV beam. Its size is proportional to the speckle size of the imaging plane. To alter the size of CV beams, we can change the distance between the HASM and the imaging plane to tune the speckle size at the imaging plane [46]. Besides, the spatial resolution of the generated CV beams is related to the pixel size of the camera, the magnification of the imaging objective O2, and the size of the generated CV beams. Apart from increasing the size of generated CV beam, employing a camera with smaller pixel size or using an imaging objective with larger magnification can help to improve the spatial resolution. In addition, the fidelity of the generated CV beams can be improved by increasing the number of degrees of freedom controlled, i.e., $M \times N$. Furthermore, instead of taking the HASM as an obstacle to overcome, HASM has been employed as an optical component to achieve polarization control [47]. By taking a HASM as a polarization modulation lens, CV beams can be created by shaping a scalar input field. In general, DMD has a fast switch rate; however, it suffers from lower efficiency—the other SLMs such as the liquid crystal SLM can be adopted to achieve high efficiency shaping of the wavefront in executing our scheme. Our method can also be used in the other highly anisotropic scattering environments, such as multimode fiber, which could benefit multimode fiber-based superresolution imaging and optical manipulation.

In summary, the correct incident wavefront for constructing CV beams through HASM can be obtained by one single scalar transmission matrix calibration in combination with an S-waveplate and a polarizer in the process of TM calibration. Compared with existing methods, the presented method only relies on manipulation of the spatial degrees of freedom of the scalar input field, which is fast and simple in terms of optical implementations and computations. As demonstrations, both radially and azimuthally polarized beams are experimentally constructed through a ZnO scattering layer. Furthermore, generalized CV beams and arrays of CV beams are created after the ZnO scattering layer to further demonstrate the flexibility of this technique. Such a method is expected to promote the applications of CV beams that involve a highly anisotropic scattering environment.

**Funding.** National Key Research and Development Program of China (2019YFA0705000); National Natural Science Foundation of China (11974218, 12004219, 12192254, 91750201, 92050202); Innovation Group of Jinan (2018GXRC010); Local Science and Technology Development Project of the Central Government (YDZX20203700001766).

**Disclosures.** The authors have no conflicts of interest to disclose.

**Data Availability.** The data that support the findings of this study are available from the corresponding authors upon reasonable request.

## REFERENCES

1. M. R. Dennis, K. O'holleran, and M. J. Padgett, "Singular optics: optical vortices and polarization singularities," in *Progress in Optics* (2009), Vol. **53**, pp. 293–363.
2. K. S. Youngworth and T. G. Brown, "Focusing of high numerical aperture cylindrical-vector beams," Opt. Express **7**, 77–87 (2000).
3. Q. Zhan, "Cylindrical vector beams: from mathematical concepts to applications," Adv. Opt. Photon. **1**, 1–57 (2009).
4. R. Dorn, S. Quabis, and G. Leuchs, "Sharper focus for a radially polarized light beam," Phys. Rev. Lett. **91**, 233901 (2003).
5. Q. Zhan and J. R. Leger, "Focus shaping using cylindrical vector beams," Opt. Express **10**, 324–331 (2002).
6. Y. Cai, W. Liu, W. Yang, J. Xu, H. Yang, and K. Shi, "Differential fluorescence microscopy by using a dynamic cylindrical-vector field," Opt. Lett. **46**, 2332–2335 (2021).
7. Y. Kozawa, D. Matsunaga, and S. Sato, "Superresolution imaging via superoscillation focusing of a radially polarized beam," Optica **5**, 86–92 (2018).

8. Q. Zhan, "Trapping metallic Rayleigh particles with radial polarization," Opt. Express **12**, 3377–3382 (2004).
9. M.-C. Zhong, L. Gong, D. Li, J.-H. Zhou, Z.-Q. Wang, and Y.-M. Li, "Optical trapping of core-shell magnetic microparticles by cylindrical vector beams," Appl. Phys. Lett. **105**, 181112 (2014).
10. Y. Kozawa and S. Sato, "Optical trapping of micrometer-sized dielectric particles by cylindrical vector beams," Opt. Express **18**, 10828–10833 (2010).
11. M. Meier, V. Romano, and T. Feurer, "Material processing with pulsed radially and azimuthally polarized laser radiation," Appl. Phys. A **86**, 329–334 (2007).
12. L. Zhang, W. Zhang, F. Lu, Z. Yang, T. Xue, M. Liu, C. Meng, P. Li, D. Mao, T. Mei, and J. Zhao, "Azimuthal vector beam exciting silver triangular nanoprisms for increasing the performance of surface-enhanced Raman spectroscopy," Photon. Res. **7**, 1447–1453 (2019).
13. M. Liu, W. Zhang, F. Lu, T. Xue, X. Li, L. Zhang, D. Mao, L. Huang, F. Gao, T. Mei, and J. Zhao, "Plasmonic tip internally excited via an azimuthal vector beam for surface enhanced Raman spectroscopy," Photon. Res. **7**, 526–531 (2019).
14. D. Pohl, "Operation of a ruby laser in the purely transverse electric mode $TE_{01}$," Appl. Phys. Lett. **20**, 266–267 (1972).
15. Y. Mushiake, K. Matsumura, and N. Nakajima, "Generation of radially polarized optical beam mode by laser oscillation," Proc. IEEE **60**, 1107–1109 (1972).
16. X.-L. Wang, J. Ding, W.-J. Ni, C.-S. Guo, and H.-T. Wang, "Generation of arbitrary vector beams with a spatial light modulator and a common path interferometric arrangement," Opt. Lett. **32**, 3549–3551 (2007).
17. W. Han, Y. Yang, W. Cheng, and Q. Zhan, "Vectorial optical field generator for the creation of arbitrarily complex fields," Opt. Express **21**, 20692–20706 (2013).
18. S. Liu, S. Qi, Y. Zhang, P. Li, D. Wu, L. Han, and J. Zhao, "Highly efficient generation of arbitrary vector beams with tunable polarization, phase, and amplitude," Photon. Res. **6**, 228–233 (2018).
19. M. Beresna, M. Gecevičius, and P. G. Kazansky, "Polarization sensitive elements fabricated by femtosecond laser nanostructuring of glass [Invited]," Opt. Mater. Express **1**, 783–795 (2011).
20. M. Beresna, M. Gecevičius, P. G. Kazansky, and T. Gertus, "Radially polarized optical vortex converter created by femtosecond laser nanostructuring of glass," Appl. Phys. Lett. **98**, 201101 (2011).
21. C. Hernández-García, A. Turpin, J. San Román, A. Picón, R. Drevinskas, A. Cerkauskaite, P. G. Kazansky, C. G. Durfee, and Í. J. Sola, "Extreme ultraviolet vector beams driven by infrared lasers," Optica **4**, 520–526 (2017).
22. M. Plöschner, T. Tyc, and T. Čižmár, "Seeing through chaos in multimode fibres," Nat. Photonics **9**, 529–535 (2015).
23. W. Xiong, C. W. Hsu, Y. Bromberg, J. E. Antonio-Lopez, R. Amezcua Correa, and H. Cao, "Complete polarization control in multimode fibers with polarization and mode coupling," Light Sci. Appl. **7**, 54 (2018).
24. H. B. d. Aguiar, S. Gigan, and S. Brasselet, "Polarization recovery through scattering media," Sci. Adv. **3**, e1600743 (2017).
25. I. M. Vellekoop, "Feedback-based wavefront shaping," Opt. Express **23**, 12189–12206 (2015).
26. D. B. Conkey, A. N. Brown, A. M. Caravaca-Aguirre, and R. Piestun, "Genetic algorithm optimization for focusing through turbid media in noisy environments," Opt. Express **20**, 4840–4849 (2012).
27. H. Li, C. M. Woo, T. Zhong, Z. Yu, Y. Luo, Y. Zheng, X. Yang, H. Hui, and P. Lai, "Adaptive optical focusing through perturbed scattering media with a dynamic mutation algorithm," Photon. Res. **9**, 202–212 (2021).
28. Z. Yaqoob, D. Psaltis, M. S. Feld, and C. Yang, "Optical phase conjugation for turbidity suppression in biological samples," Nat. Photonics **2**, 110–115 (2008).
29. Y. Liu, P. Lai, C. Ma, X. Xu, A. A. Grabar, and L. V. Wang, "Optical focusing deep inside dynamic scattering media with near-infrared time-reversed ultrasonically encoded (TRUE) light," Nat. Commun. **6**, 5904 (2015).
30. S. Popoff, G. Lerosey, R. Carminati, M. Fink, A. Boccara, and S. Gigan, "Measuring the transmission matrix in optics: an approach to the study and control of light propagation in disordered media," Phys. Rev. Lett. **104**, 100601 (2010).
31. Y.-Y. Xie, B.-Y. Wang, Z.-J. Cheng, Q.-Y. Yue, and C.-S. Guo, "Measurement of vector transmission matrix and control of beam focusing through a multiple-scattering medium based on a vector spatial light modulator and two-channel polarization holography," Appl. Phys. Lett. **110**, 221105 (2017).
32. S.-J. Tu, X. Zhao, Q.-Y. Yue, Y.-J. Cai, C.-S. Guo, and Q. Zhao, "Shaping the illumination beams for STED imaging through highly scattering media," Appl. Phys. Lett. **119**, 211105 (2021).
33. S. Tripathi, R. Paxman, T. Bifano, and K. C. Toussaint, "Vector transmission matrix for the polarization behavior of light propagation in highly scattering media," Opt. Express **20**, 16067–16076 (2012).
34. P. Yu, Q. Zhao, X. Hu, Y. Li, and L. Gong, "Tailoring arbitrary polarization states of light through scattering media," Appl. Phys. Lett. **113**, 121102 (2018).
35. A. Turpin, I. Vishniakou, and J. d. Seelig, "Light scattering control in transmission and reflection with neural networks," Opt. Express **26**, 30911–30929 (2018).
36. Y. Luo, S. Yan, H. Li, P. Lai, and Y. Zheng, "Towards smart optical focusing: deep learning-empowered dynamic wavefront shaping through nonstationary scattering media," Photon. Res. **9**, B262–B278 (2021).
37. Y. Luo, S. Yan, H. Li, P. Lai, and Y. Zheng, "Focusing light through scattering media by reinforced hybrid algorithms," APL Photon. **5**, 016109 (2020).
38. S. Tripathi and K. C. Toussaint, "Harnessing randomness to control the polarization of light transmitted through highly scattering media," Opt. Express **22**, 4412–4422 (2014).
39. I. M. Vellekoop and A. Mosk, "Focusing coherent light through opaque strongly scattering media," Opt. Lett. **32**, 2309–2311 (2007).
40. L. Gong, Y. Ren, W. Liu, M. Wang, M. Zhong, Z. Wang, and Y. Li, "Generation of cylindrically polarized vector vortex beams with digital micromirror device," J. Appl. Phys. **116**, 183105 (2014).
41. J. Yang, Q. He, L. Liu, Y. Qu, R. Shao, B. Song, and Y. Zhao, "Anti-scattering light focusing by fast wavefront shaping based on multi-pixel encoded digital-micromirror device," Light Sci. Appl. **10**, 149 (2021).
42. D. Wang, E. H. Zhou, J. Brake, H. Ruan, M. Jang, and C. Yang, "Focusing through dynamic tissue with millisecond digital optical phase conjugation," Optica **2**, 728–735 (2015).
43. W.-H. Lee, "Binary computer-generated holograms," Appl. Opt. **18**, 3661–3669 (1979).
44. B. Perez-Garcia, C. López-Mariscal, R. I. Hernandez-Aranda, and J. C. Gutiérrez-Vega, "On-demand tailored vector beams," Appl. Opt. **56**, 6967–6972 (2017).
45. S. Popoff, G. Lerosey, M. Fink, A. C. Boccara, and S. Gigan, "Image transmission through an opaque material," Nat. Commun. **1**, 81 (2010).
46. E. Edrei and G. Scarcelli, "A trade-off between speckle size and intensity enhancement of a focal point behind a scattering layer," Sci. Rep. **9**, 11256 (2019).
47. J.-H. Park, C. Park, H. Yu, Y.-H. Cho, and Y. Park, "Dynamic active wave plate using random nanoparticles," Opt. Express **20**, 17010–17016 (2012).